Poly(3-hydroxybutyrate) and Poly(3-hydroxyoctanoate) Blends: Morphology and Mechanical Behavior

Alain Dufresne*,† and Marc Vincendon‡

Centre de Recherches sur les Macromolécules Végétales (CERMAV-CNRS), Université Joseph Fourier, BP 53, 38041 Grenoble Cedex 9, France; and Institut Universitaire de Technologie, Département de Chimie-Matériaux, 39, Bd Gambetta, 38000 Grenoble, France

Received November 2, 1999

ABSTRACT: Blends of bacterial poly(hydroxybutyrate) (PHB) with poly(hydroxyoctanoate) (PHO) were prepared by co-dissolving the two polyesters in chloroform and casting the mixture. To probe the question of blend miscibility, scanning electron microscopy (SEM) observations and differential scanning calorimetry (DSC) spectra were collected for the blends and blend components as well. It has been observed that PHB shows no miscibility at all with PHO, resulting in two-phase systems in which the nature of the continuous phase is composition-dependent. Dynamic mechanical analysis and tensile properties of these materials were also investigated. The morphology of the blend strongly influences the mechanical behavior. The mechanical properties of these materials have been predicted from a model involving the percolation concept. It takes both linear and nonlinear mechanical behaviors into account and allows for the effect of the lack of adhesion between material domains and/or breakage of one of the component.

Introduction

Because poly(3-hydroxybutyrate) (PHB) is very brittle and prone to thermal degradation, it is necessary to improve its mechanical properties and processability through copolymerization or blending. In fact, since it is very costly to develop new copolymers, blending with a second, already existing polymer has been attempted by a number of investigators.

There have been numerous reports on the blending of PHB with other biodegradable polymers or with polymers that are refractory to biodegradation. Polymers, which have been found to be miscible with PHB, include poly(vinyl acetate) (PVAc),[1,2] poly(epichlorohydrin) (PECH),[3,4] poly(vinyl alcohol) (PVA),[5] atactic poly[(R,S)-3-hydroxybutyrate],[6] and its block copolymer with poly(ethylene glycol) (P(*R*,*S*−HB-*b*-EG),[7] poly(L-lactic acid-*co*-ethylene glycol-*co*-adipic acid),[8] poly(vinylidene fluoride) (PVDF),[9,10] cellulose acetate butyrate (CAB) or cellulose acetate propionate (CAP),[11] and poly(ethylene oxide) (PEO).[12,13] Poly(methyl methacrylate) (PMMA) is known to be immiscible with PHB at room temperature,[14] however, it is partially miscible in its molten state.[15] Immiscible blends have been prepared by mixing PHB with poly(1,4-butylene adipate) (PBA),[2] poly(ϵ-caprolactone) (PCL),[2] poly(cyclohexyl methacrylate) (PCHMA),[15] poly(3-hydroxybutyrate-*co*-valerate) (P(HB−HV)),[16−21] and rubbers, such as ethylene-propylene rubber (EPR),[1,22] ethylene−vinyl acetate (EVA),[12,22] modified EPR rubbers, grafted with succinic anhydride (EPR-*g*-SA) or dibutyl maleate (EPR-*g*-DBM), or a modified EVA polymer containing OH groups (EVAL).[22] Verhoogt et al.[23] wrote a review article on the properties and biodegradability of blends containing either PHB or P(HB−HV).

In the present paper the results of an investigation concerning the morphology, thermal and mechanical behavior of blends obtained by co-dissolving and mixing PHB with poly(hydroxyoctanoate) (PHO) are reported. Only a few studies on blend systems composed of two crystalline polymers have been reported[9,10,20,24,25] and in most cases, the miscibility of the blends is questionable. It is very difficult to analyze the miscibility of such blends, because miscibility is a property of the amorphous phase, and the existence of the crystalline phase prevents the observation of the amorphous phase. For example, it is difficult to observe precise glass transition temperatures (T_g) of blends with relatively high crystallinity. Thus, it is not easy to assess miscibility of such polymer blends from T_g data, the existence of the crystalline phase increasing the apparent T_g. Of particular interest is the relationship between blend morphology and physical properties. One of the goal of this study is to find out if blending PHB with PHO may influence the impact properties of the former at low temperature.

Experimental Section

Materials. PHO used in this study was kindly supplied by Dr. E. Samain, CERMAV, and has been obtained by fermentation of *Pseudomonas oleovorans* (ATCC 29347). The bacterial strain and growth conditions were described elsewhere.[6] The typical monomer composition of PHA produced by sodium octanoate grown cells has already been described.[26] *P. oleovorans* produces a random copolymer composed of mostly of C8 and smaller amounts of C6 and C10 monomers when fed on octanoate. The octanoate content was shown to be of about 86%. In addition, it was reported that changing growth conditions did not have a significant influence on the monomer composition of the PHA produced with sodium octanoate.[26]

* To whom correspondence should be addressed (e-mail: Alain.Dufresne@cermav.cnrs.fr).
† CERMAV−CNRS.
‡ Institut Universitaire de Technologie.

10.1021/ma991854a CCC: $19.00
Published on Web 03/29/2000

After reaching the early stationary growth phase, the cells were harvested by centrifugation (20 min, 7000 rpm), and the biomass was freeze-dried. Intracellular PHO was extracted from the freeze-dried cells by refluxing in chloroform as described elsewhere.[27] After a reflux period of 72 h, the solution was filtered and concentrated by evaporation at 35 °C. The remaining residue was precipitated into vigorously stirred and ice-kept methanol. The methanol volume should be at least 10 times higher than the polymer volume. PHO was collected by filtration and dried under vacuum for 48 h at 40 °C.

PHB was kindly supplied as a white powder by Monsanto Europe S. A. (Belgium). It was used as received.

Film Processing. PHB/PHO blends were obtained by dissolving each constituent in chloroform as follows. PHB was first dissolved in chloroform (10 wt %) under stirring for 8 min at 70 °C. PHO was subsequently added into the flask. The PHO amount was adjusted, depending on the blend composition, to obtain a final polymer weight of 1.35 g. Further chloroform was added to keep a constant 10 wt % concentration. The solution was stirred for 8 min at 70 °C and constant polymer concentration to ensure complete dissolution of both components. Additional heating for 5 min at 70 °C allowed concentrating the solution by partial evaporation of chloroform. The solution was then kept at room temperature for 2 min and in a ground-ice bath for 15 min. This latter step was important to avoid cracking of films. The solution was subsequently stored at room temperature for 20 min and vigorously stirred, and the resulting viscous solution was cast in a Teflon mold (2 × 7 mm) and dried at room temperature until the film was formed. Films were allowed to age at room temperature for at least 2 weeks, to let them reach a stabilized crystallinity before testing. Blend compositions are indicated throughout this work as weight ratios of PHB/PHO and were varied from 100/0 (pure PHB) up to 0/100 (pure PHO).

FT-IR Measurement. FT-IR spectra of blend films were recorded on a Perkin-Elmer 1720X spectrometer by transmission method at room temperature in the range from 4000 to 400 cm^{-1} at a resolution of 4 cm^{-1}.

Nuclear Magnetic Resonance. Solid-state high-resolution ^{13}C NMR spectra were obtained on a Brüker MSL spectrometer at 50 MHz. The CP/MAS and SP/MAS modes were employed depending on the mobility of the observed phase.

^{1}H NMR spectra were recorded on a Brüker AC 200 MHz spectrometer in deutered chloroform ($CDCl_3$).

Scanning Electron Microscopy. Scanning electron micrographs (SEM) were obtained on a JEOL JSM-6100 scanning electron microscope. All specimens were submerged into liquid nitrogen, fractured, and then sputter coated with a thin layer of gold on a JEOL JFC-1100E ion sputter coater before SEM observations. SEM micrographs were obtained using 7 kV secondary electrons.

Differential Scanning Calorimetry. Differential scanning calorimetry (DSC) was performed with Perkin-Elmer DSC7 equipment, fitted with a cooler system using liquid nitrogen. It was calibrated with an indium standard. Scans were performed at least 2 weeks after film formation to ensure stabilization of the degree of crystallinity and perfect reliability of measurements. At least three individual measurements were made to ensure reproductibility.

Each sample was heated from −80 to +220 °C at a heating rate of 20 K/min (first scan corresponding to cast films). Subsequently, they were quenched to −80 °C. Second scan heating curves (corresponding to quenched films) were then collected by heating from −80 to +220 °C at 20 K/min. The melting temperature (T_m) was taken as the peak temperature of the melting endotherm while the glass transition temperature (T_g) was taken as the inflection point of the specific heat increment at the glass−rubber transition.

Dynamic Mechanical Analysis. Dynamic mechanical tests were accomplished using a Rheometrics RSA2 spectrometer in the tensile mode. Test conditions were chosen in such a way that the measurements were in the linear viscoelasticity region (the maximum strain ϵ was around 10^{-4}). The specimen was a thin rectangular strip with dimensions of 30 × 3 × 1 mm. The setup measured the complex tensile modulus E^*, i.e., the storage component E' and the loss component E'', as well as the ratio of the two components, i.e., tan ϕ ($=E''/E'$). In the present work, results are displayed through E' and E''. Measurements were performed in isochronal conditions at 1 Hz, and the temperature was varied by steps of 3 K from 175 to 450 K.

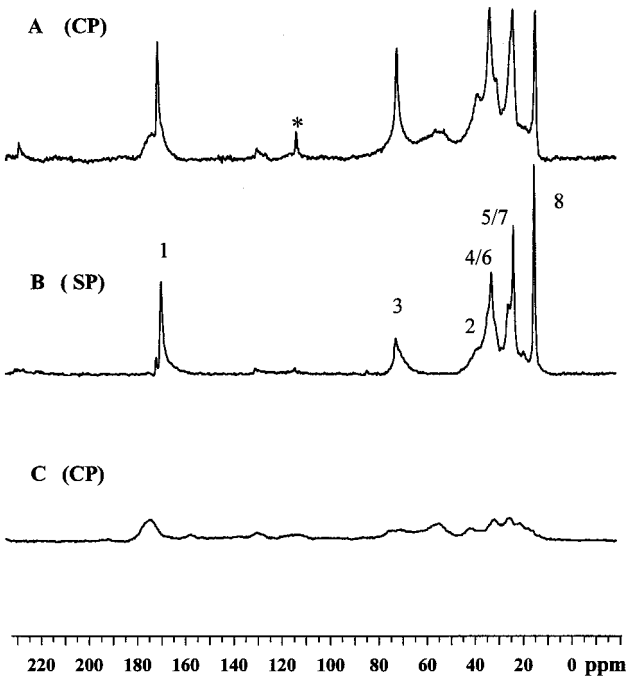

Figure 1. High-resolution solid-state ^{13}C NMR spectra: (A) culture cells from *P. oleovorans*, cross polarization spectrum (CP); (B) culture cells from *P. oleovorans*, single pulse spectrum (SP); (C) culture cells after chloroform extraction (CP). ∗ = spinning band.

Tensile Tests. The nonlinear mechanical behavior was analyzed using an Instron 4301 testing machine in tensile mode, with a load cell of 100 N capacity. The specimen was a thin rectangular strip (∼30 × 5 × 0.5 mm). The stress−strain curves of solution-cast films of PHB/PHO blends were obtained at 25 °C at a strain rate $d\epsilon/dt = 8.33 \times 10^{-3}$ s^{-1} (cross-head speed = 10 mm/min) and a gauge length of 20 mm. The true strain ϵ can be determined by $\epsilon = \ln(L/L_o)$, where L and L_o are the length during the test, and the length at zero time, respectively. The true stress σ was calculated by $\sigma = F/S$, where F is the applied load and S is the cross-sectional area. The calculation of these data was performed assuming constant volume behavior. Stress vs strain curves were plotted and Young's modulus (E) was measured from the low strain region.

Ultimate mechanical properties were also characterized. The true ultimate stress, or true stress at break, $\sigma_b = F_b/S$, where F_b is the applied load at break, was reported for each tested sample. Ultimate elongation was characterized by the true ultimate strain, or true strain at break, $\epsilon_b = \ln [1 + (\Delta L_b/L_o)]$, where ΔL_b is the elongation at break. The mechanical tensile data were determined on average of at least three specimens.

Results and Discussion

PHO Characterization. Figure 1 shows the high-resolution solid-state ^{13}C NMR spectra of the cells produced by *P. oleovorans* (Figure 1A). On this spectrum, one can observe six thin signals arising from the mobile chains of PHO superimposed to broad signals arising from the bacteria. It is possible to obtain direct polarization spectra in the solid state via single-pulse technique (SP), which will reveal relatively mobile

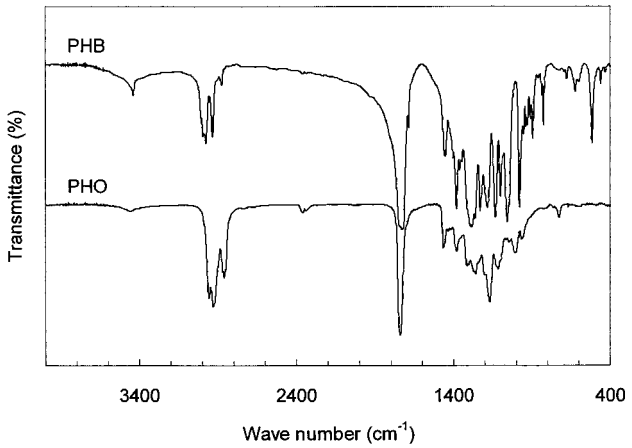

Figure 2. Infrared spectra of PHB and PHO obtained on films.

chains or chain segments. Figure 1B shows the ^{13}C NMR SP spectrum and visualizes signals of the more mobile carbon of the PHO chain. On this spectrum, the carbon signals are assigned to the monomeric repeating unit of PHO according to already published results.[28] Figure 1C shows the high-resolution ^{13}C NMR CP/MAS spectrum of the residual cells, after solvent extraction of the PHO, yielding only broad signals.

The extracted PHO, after purification by precipitation from a chloroform solution, was first characterized via infrared spectroscopy. Figure 2 shows the infrared spectra for films of PHO as well as for the commercial PHB. Discrimination between the two polymers can be made on the 720 cm^{-1} methylene chain vibration band of PHO.

^1H and ^{13}C NMR spectra of purified PHO were obtained in deuterated chloroform solutions and were found to be in agreement with published data.[36] It is noticed that the solution ^{13}C NMR spectrum indicates the presence of small signals (10%) due to nonoctanoate units.

Morphological Characterization of Films. Examination of the surfaces of fractured films obtained from solution-cast PHB/PHO blends were carried out using SEM. Before analyzing the morphology of blends, fractured surfaces of both parent polymers were studied. Figure 3 shows the surface of pure PHB (Figure 3a) and pure PHO (Figure 3b) films, just after fracture. The freshly fractured surface of PHB film is chaotic and exhibits a bristled openwork polymeric network. On the other hand, the fractured surface of PHO film is smooth and only a few fermentation byproducts emerge. The difference between both polymers is most likely due to their difference in crystallinity.

Figure 4 shows the fractured surface of 80/20, 50/50, and 20/80 blends. The higher the PHB content, the rougher the surface of fracture appears. By comparison of the micrographs of Figures 3 and 4, it seems that this phenomenon could be due to the phase separation between PHB and PHO. In Figure 4a, the bristled openwork PHB network is easily seen, and PHO domains appear as "marbles" or beads, whose size and distribution are very irregular. This is an indication that PHB and PHO form mainly a two phase-system, in which the continuous phase of the 80/20 blend is formed by PHB and the inclusions (bead-shaped) are PHO domains. These beads, which range between 1 and 10 μm in size, are embedded in PHB, and the adhesion between both polymer domains appears to be very weak,

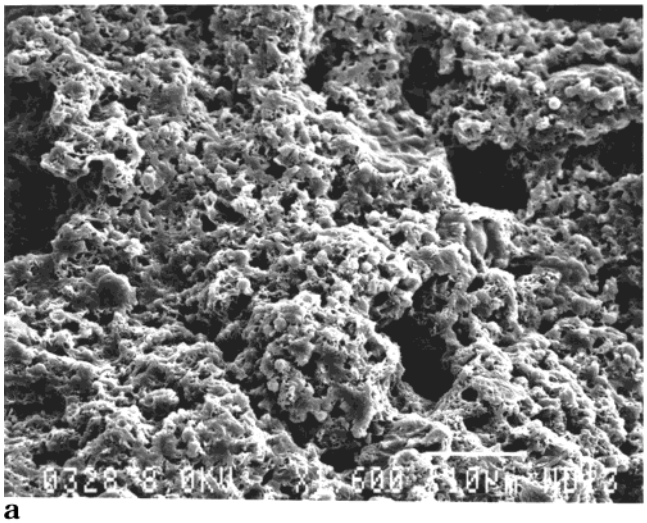

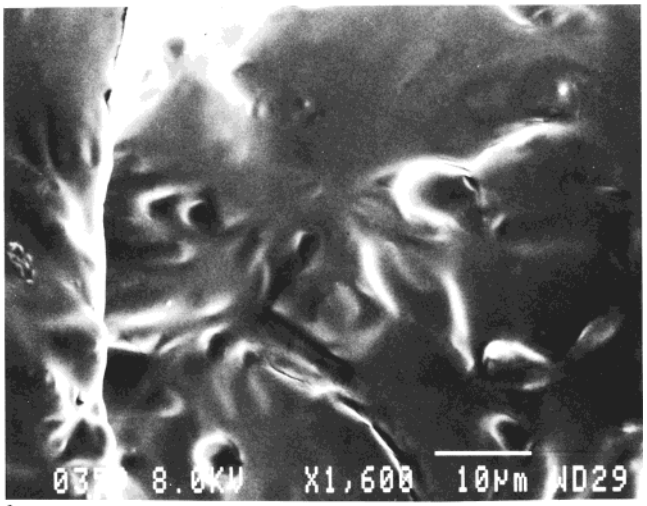

Figure 3. Scanning electron micrographs showing the freshly fractured surface of (a) pure PHB (100/0) and (b) pure PHO (0/100).

as displayed by the space located at the interface. Increasing the PHO content (Figure 4b) induces an increase of the appearance of smooth polymeric domains. For this composition (50/50), it seems that cocontinuous PHB and PHO phases coexist. The openwork PHB network is partially filled by PHO and distinct phase segregation is seen. For the PHO-rich blend (20/80, Figure 4c), the fractured surface is smooth and similar to the one or pure PHO (Figure 3b). Poorly dispersed PHB domains appear as protuberances, and it is obvious that the continuous phase is PHO for this composition.

Thermal Analysis. Differential scanning calorimetry (DSC) measurements were performed to characterize the solution-cast films of PHB/ PHO blends. Figure 5 shows the DSC traces of PHB and its blends with PHO. Figure 5a corresponds to the DSC thermograms collected during the first heating scan (cast films), whereas Figure 5b corresponds to the second heating scan (quenched films) (see Experimental Section).

The melting thermogram of pure cast PHB (Figure 5a) exhibits a shoulder around 165 °C and an endothermal peak around 180 °C. The shoulder is attributed to the melting of the semicrystalline film as cast. An exothermal peak arising from the recrystallization

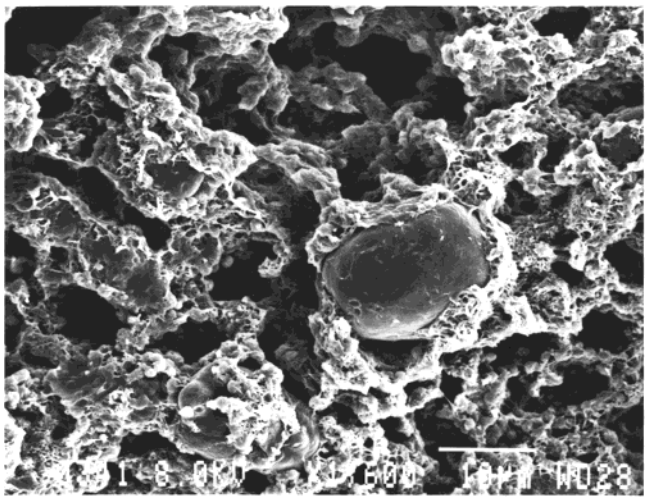

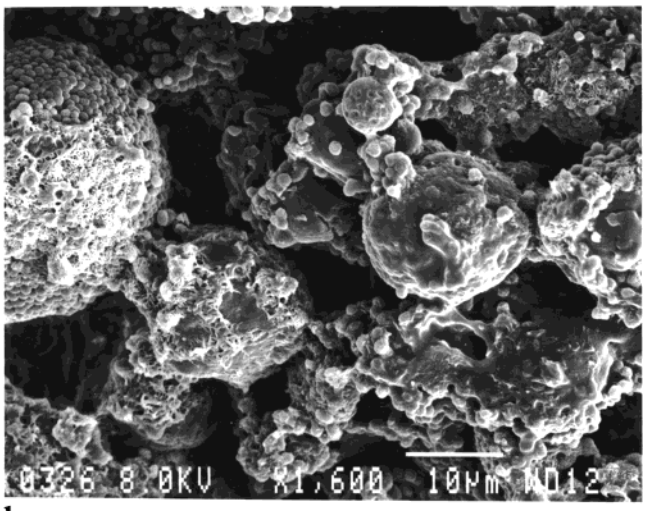

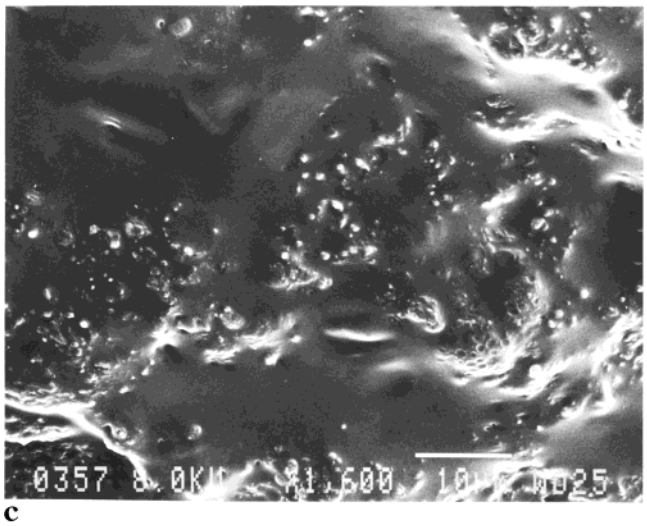

Figure 4. Scanning electron micrographs showing the freshly fractured surface of (a) 80/20, (b) 50/50, and (c) 20/80 blends.

during the heating should exist between the shoulder and the endothermal peak. The endothermal peak appearing at 180 °C is attributed to the melting of the recrystallized component.[30] After the sample is quenched to −80 °C, the second scan (Figure 5b, quenched films) exhibits a specific heat increment around 5 °C ascribed to the glass−rubber transition of PHB. At higher

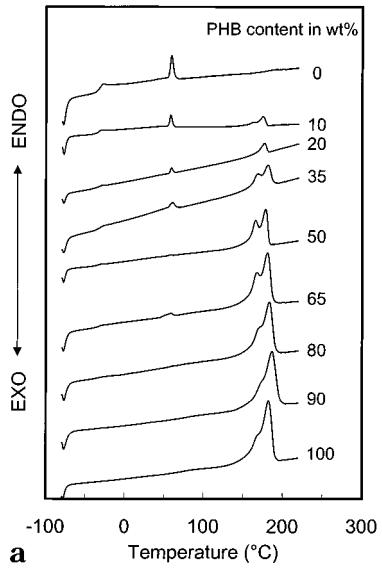

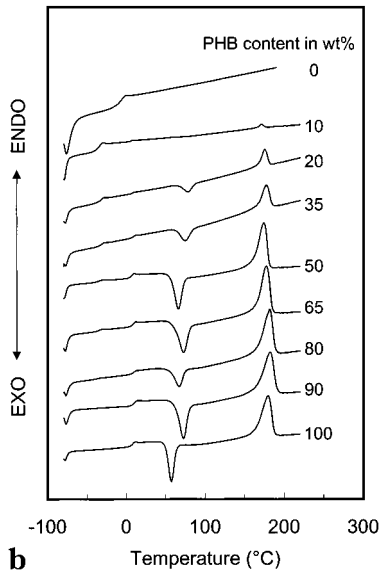

Figure 5. DSC thermograms of PHB, PHO, and various PHB/PHO blend films as cast (a) and after melt quenching (b). The compositions are indicated in the figure.

temperature, an exothermal peak around 60 °C corresponding to the crystallization of PHB is observed. The melting of these nonisothermally crystallized domains occurs around 180 °C. It is worth noting that the melting endotherm of the quenched PHB displays a single peak without any shoulder. Pure PHO cast film exhibits an endothermal baseline shift around −35 °C (Figure 5a) associated with the glass−rubber transition. This value agrees with previously reported T_g values for PHO.[27,31−33] The observation of the glass−rubber transition for cast PHO arises from the fact that the crystallinity is much lower than for PHB. Around 60 °C, an endothermal peak displays the melting of PHO. The second heating scan (Figure 5b) exhibits only the glass−rubber transition, owing to the low kinetic of crystallization of PHO.[34] The DSC traces of the various PHB/PHO blends consist in a superimposition of the thermograms of the two parent polymers balanced by the composition. However, for intermediate compositions (65/35, 50/50, and 35/65 blends) the low-temperature melting peak of PHB is better resolved and higher relative to the high-temperature peak.

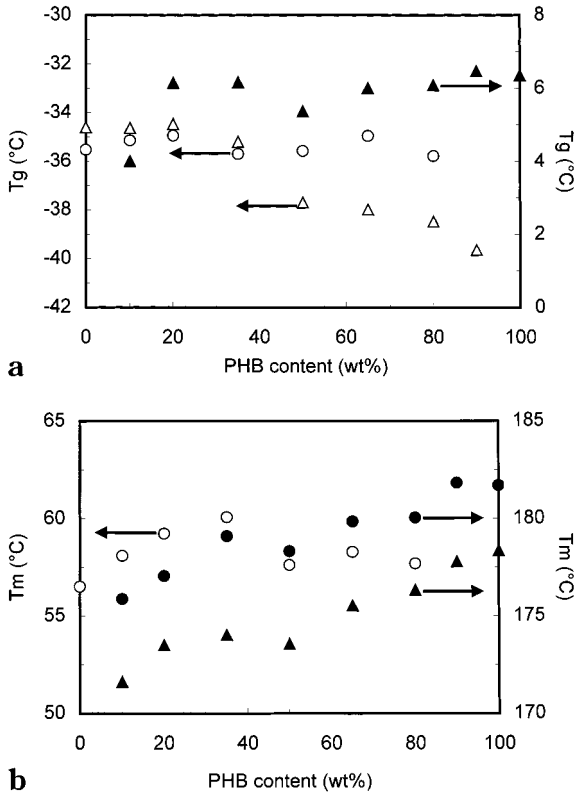

Figure 6. Temperature of the transitions of various PHB/PHO blends vs PHB content, using data obtained from the DSC curves shown in Figure 5: (a) glass transition and (b) melting temperature of the (●) PHB phase of cast films, (▲) PHB phase of quenched films, (○) PHO phase of cast films, and (△) PHO phase of quenched films.

The temperatures of the calorimetric transitions of the PHB/PHO blends, taken from the curves of Figure 5, are plotted in Figure 6 as a function of composition. The blends show two distinct T_g values in DSC measurements (Figure 6a): the first one, at about −35 °C, for the PHO phase and the second one, at about 6 °C, for the PHB phase. This latter transition was observed only for the quenched samples. Almost no dependence on composition is observed. This finding strongly suggests that PHB and PHO are immiscible in the amorphous state. However, it is observed that quenched samples display a weak depression of T_g of the PHO phase up to −40 °C for PHB-rich blends. This could be ascribed to an increase in the molecular mobility of amorphous PHO chains in the presence of amorphous quenched PHB.

Figure 6b shows the variation of the melting temperature against composition for both the PHO and the PHB phases. No melting-point was observed for the PHO phase in quenched films. The T_m value of PHB phase for both cast and quenched films decreases slightly from 182 to 176 °C and from 178 to 172 °C, respectively, as the PHB content in the blend decreases from 100 to 10 wt %. This phenomenon could be related to a decrease of the PHB crystallites size in the presence of PHO. Indeed, the PHB spherulites grow in the presence of a PHB melt containing PHO domains as the dispersed phase. During growth the PHO particles are probably first ejected and then occluded in interspherulitic regions according to a mechanism already described by Greco and Martuscelli[1] for PHB/EPR blends. An increase in the PHO content could therefore results in an increase in this phenomenon, and in a decrease of the PHB spherulites. No depression of the melting-point was reported for the PHO phase.

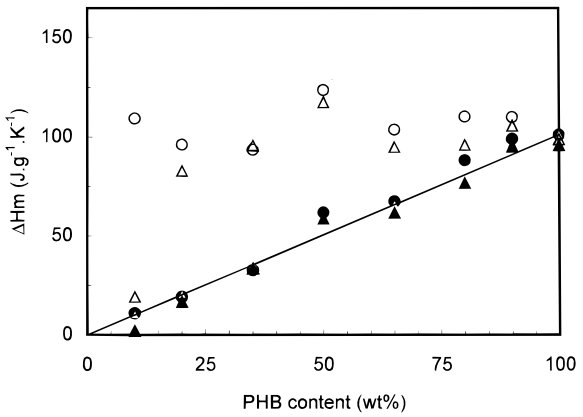

Figure 7. Heat of fusion of PHB vs PHB content: per gram of blend in (●) cast films and (▲) quenched films and per gram of PHB in the blend in (○) cast films and (△) quenched films. The solid line corresponds to the theoretical value.

Figure 7 shows the plot of the apparent enthalpy of fusion per gram of blend (ΔHm) for the PHB phase in the PHB/PHO blend films against the PHB content in the blends for both cast (filled circles) and quenched samples (filled triangles). It decreases nearly linearly as the PHB content in the blend decreases, as expected. The solid line corresponds to the theoretical value of the apparent enthalpy of fusion defined as the product of the enthalpy of fusion of the cast pure PHB and the weight fraction of PHB in the blend. A good agreement is found between experimental data and theoretical prediction. This result suggests that the crystallinity ratio of PHB is not influenced by blending with PHO.

The heat of fusion per gram of PHB in the blend was also reported in Figure 7 for both cast (open circles) and quenched samples (open triangles). It is almost composition-independent. The crystallinity of PHB phase is therefore practically not influenced by blend composition, except for the 10/90 quenched blend.

Dynamic Mechanical Analysis. Dynamic mechanical measurements were performed on all the samples, including parent polymers. Figure 8 shows a plot of log(E'/Pa) (Figure 8a) and log(E''/Pa) (Figure 8b) at 1 Hz as a function of temperature for various solution-cast films of PHB/ PHO blends. For the sake of clarity, each curve was shifted by 1 decade with regard to the previous one, pure PHO being the reference.

Both parent polymer display typical behaviors of semicrystalline polymers. At low temperature the amorphous part of the polymer is in the glassy state, and the modulus slightly decreases with temperature but remains roughly constant (around 2 GPa). Then, a rapid decrease in the elastic tensile modulus, by more than 1 decade is observed for PHO in the range 230−260 K. It appears in the glass−rubber transition zone previously determined by DSC. This modulus drop is therefore ascribed to an energy dissipation phenomenon involving cooperative motions of long amorphous chain sequences. It is displayed in Figure 8b in the concomitant relaxation process where the loss modulus passes through a maximum at ∼240 K. The rubbery modulus is known to depend on the degree of crystallinity of the material. The crystalline domains act as both physical cross-links and filler particle due their finite size, and would increase the modulus of the semicrystalline polymer. No

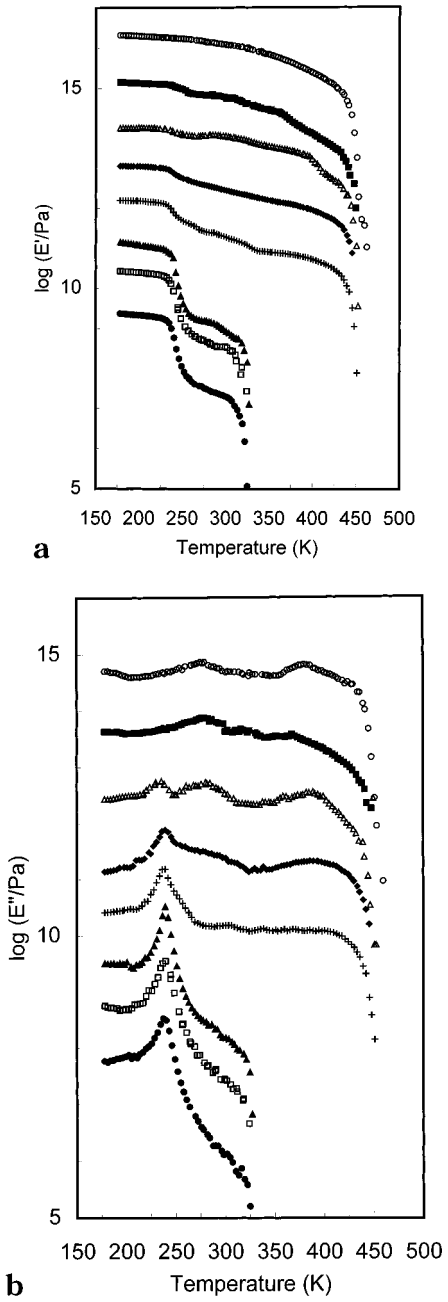

Figure 8. (a) Logarithm of the storage tensile modulus E' and (b) logarithm of the loss tensile modulus E'', vs temperature at 1 Hz for blends 100/0 (○, pure PHB), 90/10 (■), 80/20 (△), 65/35 (◆), 50/50 (+), 20/80 (▲), 10/90 (□), and 0/100 (●, pure PHO). Scales correspond to curves 0/100. Other curves (10/90−100/0) are shifted by 1 decade for the sake of clarity.

storage modulus drop is observed in the glass−rubber transition zone of pure PHB (∼280 K), due to its high degree of crystallinity. However, this transition is displayed through an ill-defined relaxation process at ∼280 K (Figure 8b). At higher temperature, the storage modulus drops irremediably with the breakup of crystalline domains, around 330 and 450 K for PHO and PHB, respectively. These values are in good agreement with melt temperatures measured by DSC.

For the various blend compositions, the viscoelastic behavior should be the superimposition of the viscoelastic behavior of both parent polymers, balanced by the volume fraction of each constituent. For each specimen, a relaxation process associated with the glass−rubber transition of PHO and the concomitant modulus drop are observed in the range 230−260 K, which magnitude decreases as the PHB content increases. In the same way, the ill-defined peak ascribed to T_g of PHB appears around 280 K as the PHB content in the blend increases. For the blends containing 50 up to 100 wt % PHB, an additional peak is observed in the range 350−425 K in the E'' spectra. It is ascribed to the viscoelastic behavior of amorphous polymeric chains flowing by diffusion within the surrounding entangled network and crystalline PHB domains. An interpretation of this relaxation process in poly(methyl methacrylate) (PMMA) was proposed on physical basis.[35] The evolution of the E'' peak ascribed to T_g is of major interest because, as mentioned in the Introduction, the glass transition is not easily perceptible by DSC, as is the case for most semicrystalline polymers. Indeed, the study of this transition and more precisely of the temperature at which E'' reaches its maximum, can display possible miscibility phenomena. We ascertain in Figure 8b that the temperature position of the E'' peak associated with T_g of PHO is unaffected by blending with PHB and remains composition-independent.

Modeling of the Viscoelastic Behavior. To relate the microstructure and the mechanical behavior of PHB/PHO blends, the modeling of the viscoelastic properties of the materials and comparison with experimental data is a powerful tool. In multiphase polymer systems, the relationship between the elastic moduli, the composition of the two components, and the morphologies (or geometrical arrangement of each phase) has been extensively studied. Different models can be used to predict the elastic behavior of two-phases systems such as blends of amorphous polymers.[36−44] Most theories assume perfect adhesion between phases and the sample being macroscopically homogeneous and isotropic. In fact, it has been shown that the materials processed for this study are four-phase systems, PHB and PHO being semicrystalline polymers. Because it is very difficult to derive a model for such composite systems, it is of interest to consider the following hypothesis. At temperatures between their T_g and their melting point, semicrystalline polymers are often considered as soft matrixes reinforced by crystallites. Their mechanical behavior as well as T_g of their amorphous phase mainly depend on the crystallinity ratio, the average crystallite size, and the interface between the crystalline phase and the amorphous phase. However, on the scale of 1 μm, i.e., the average size of inclusion dimensions in our blends, if no specific orientation occurs during processing, the behavior of most semicrystalline polymers can be considered as homogeneous and isotropic. Accordingly, for modeling the mechanical behavior of the blends they may be considered as two-phase systems, each phase being an homogeneous phase which has the same macroscopic behavior as PHB or PHO.

Furthermore, the behavior of polymers is not purely elastic but is in fact viscoelastic.[45] For this reason, it is usual to modify the relationships for elasticity in introducing viscoelastic moduli (for each phase), i.e., under their complex form $E^*(i\omega,T)$.[39] In previous works, a series-parallel model as proposed by Takayanagi,[37] in which the concept of percolation was introduced,[42] gave successful results when applied to cellulose/PA66,[43] cellulose/PA6,69,[46] and chitosan/PA6 blends.[44] The Takayanagi prediction is a phenomenological model which consists of a mixing rule between the two simplest models involving connections in series (Reuss prediction)

or in parallel (Voigt prediction) of the components. However, it was shown that for blends involving semicrystalline polymers, a better prediction of the mechanical behavior can be performed by using a "three-branch" model rather than the classical "two-branch" model.[43,44,46]

Under a tensile situation the predicted complex modulus, E^*, of the "three-branch" model is given by (see ref 43 for the full calculation)

$$E^* = \psi_O E_H^* + \frac{(1-\psi_H-\psi_O)^2 E_H^* E_O^*}{(1-\psi_H-v_O)E_O^* + (v_O-\psi_O)E_H^*} + \psi_H E_H^* \quad (1)$$

where E_H^* and E_O^* correspond to the experimental complex tensile modulus of PHB and PHO, respectively, ψ_H and ψ_O are the volume fraction of the PHB and PHO phase which has percolated, i.e., which presents a continuity within the blend, and $v_O = v_H - 1$ is the volume fraction of the PHO phase (v_H being the volume fraction of the PHB phase). Considering v_{Hc} and v_{Oc} as the critical volume fraction of PHB and PHO phases, respectively, at the percolation threshold, and b_H and b_O the corresponding critical exponents, $\psi_{H(O)}$ can be written as:

$$\begin{bmatrix} \psi_{H(O)} = v_{H(O)}\left[\dfrac{v_{H(O)} - v_{H(O)c}}{1 - v_{H(O)c}}\right]^{b_{H(O)}} & \text{for } v_{H(O)} > v_{H(O)c} \\ \psi_{H(O)} = 0 & \text{for } v_{H(O)} < v_{H(O)c} \end{bmatrix} \quad (2)$$

which are consistent with the fact that ψ_H and ψ_O should be equal to 1 when v_H and $v_O = 1$, respectively.

It follows from eq 1 that the expressions of E' and E'' given in the Appendix correspond to the complete three-branch model, which will be labeled the 3B model after this. Though it is difficult to determine v_{Hc}, v_{Oc}, b_H, and b_O (eq 2) as they depend on many parameters such as the geometry and the spatial distribution of each phase, we have considered that $v_{Hc} = v_{Oc} = 1 - v_{max}$, where v_{max} is the maximum volume fraction of rigid isoradius spheres, so that $v_{Hc} = v_{Oc} \approx 0.25$. The critical exponents b_H and b_O of the probability to obtain an infinite cluster are about 0.4 for the random sites percolation model.[47,48] The application of this model requires the knowledge of the experimental mechanical behavior of the pure parent components: PHB and PHO.

Depending on the composition and then on the morphology of the blend, various arrangements of the three-branch model can be considered. One of the simplest models involves connections in series (Reuss prediction) or in parallel (Voigt prediction) of the components, and leads to the lowest lower bound or the highest upper bound for the moduli, respectively. This highest upper bound is applicable to a material in which two components are connected in parallel to the direction of the applied force. The lowest lower bound of the modulus is related to the model in which the two phases are connected in series, perpendicular to the applied force.

Other possibilities consist in connecting in parallel the Reuss model and a volume fraction, ψ_H or ψ_O, of the percolating PHB or PHO phase, respectively. This leads to the predictions which will be labeled the two-branch H (2BH) model or the two-branch O (2BO) model, respectively, in the present study.

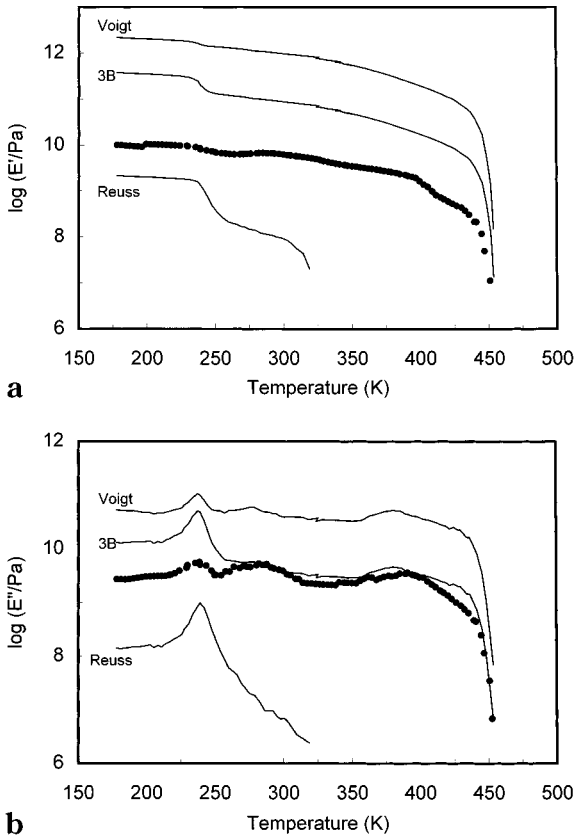

Figure 9. Experimental data (●) and predicted data (—) from various models for (a) the storage tensile modulus and (b) the loss tensile modulus, vs temperature at 1 Hz of the blend 80/20. Scales correspond to curves predicted from the Reuss model. Other curves are shifted by 1 decade for the sake of clarity.

Calculated and experimental data are shown in Figures 9−11 for 80/20, 50/50, and 20/80 cast-blends, respectively. The calculated storage and loss moduli from the various predictions are shown in parts a and b of Figure 9, respectively, for the 80/20 blend, which also show experimental results (filled circles). For this composition, the predictions of both Reuss and 2BO models are equivalent, because the volume fraction of PHO phase is lower than the percolation threshold v_{Oc}. The same observation can be reported for both 3B and 2BH predictions. Therefore, the predictions of both 2BO and 2BH models are not plotted in Figure 9. It is clearly seen in Figure 9 that the fit is unsatisfactory in the case of the Reuss model. This is an indication that a continuous PHB phase is present in the blend. This phenomenon is in good agreement with the observations by SEM (see Figure 4a). The two other calculated curves are nearly in good agreement with experimental data over the whole temperature range. The difference between these two sets of models is the presence or the absence of the percolating PHO phase, which plays a minor part on the mechanical behavior of the blend, especially at high temperature. However, these models fail to describe the relaxation corresponding to T_g of both PHO and PHB phases. The experimental storage modulus drop and associated maximum in loss modulus ascribed to T_g of PHO (~240 K) are not as well defined as predicted ones. On the contrary, the experimental mechanical relaxation process corresponding to T_g of PHB is more distinct than the calculated one.

The calculated and experimental data for the storage and loss components of the complex tensile modulus vs

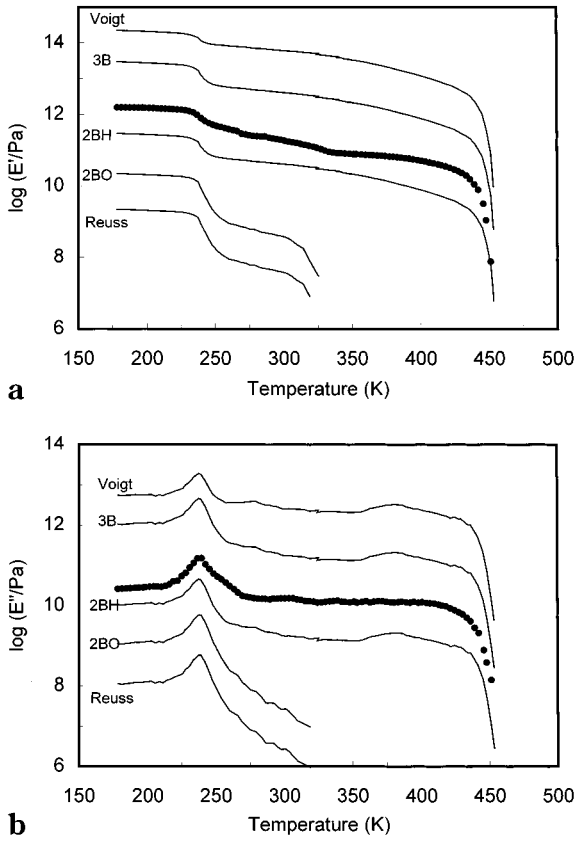

Figure 10. Experimental data (●) and predicted data (—) from various models for (a) the storage tensile modulus and (b) the loss tensile modulus, vs temperature at 1 Hz of the blend 50/50. Scales correspond to curves predicted from the Reuss model. Other curves are shifted by 1 decade for the sake of clarity.

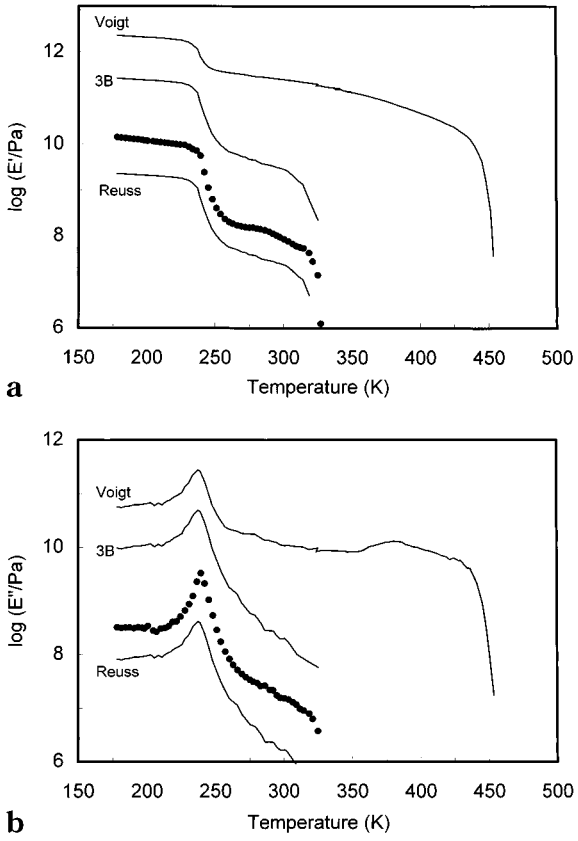

Figure 11. Experimental data (●) and predicted data (—) from various models for (a) the storage tensile modulus and (b) the loss tensile modulus, vs temperature at 1 Hz of the blend 20/80. Scales correspond to curves predicted from the Reuss model. Other curves are shifted by 1 decade for the sake of clarity.

temperature are shown in parts a and b of Figure 10, respectively, for the 50/50 blend. The experimental behavior is well predicted from the Voigt model, as well as from the 3B and 2BH models. On the contrary, the Reuss and 2BO predictions fail to fit the experimental data. This is a good indication that the PHB domains percolate and form a continuous phase for this PHB/PHO composition.

For the 20/80 blend (Figure 11), the predictions of both Reuss and 2BH models are equivalent, because the volume fraction of the PHB phase is lower than the percolation threshold v_{Hc}. The same observation can be reported for both 3B and 2BO predictions. Therefore, the predictions of both 2BO and 2BH models are not plotted in Figure 11. The experimental mechanical behavior of the 20/80 blend is fairly well predicted from the Reuss and 3B models, whereas the Voigt model fails to fit it. This suggests, in agreement with SEM observations (Figure 4c), that PHO forms the continuous phase.

In addition, it is worthwhile to note that the temperature positions of the experimental relaxation processes associated with T_g of both the PHB and PHO domains are well predicted by the various models. This is a good indication of a total lack of miscibility between both components.

High Strain Behavior. Thermal and thermomechanical measurements discussed above have displayed total immiscibility between both homopolymers in the blend. This should lead to a poor adhesion between phases and result in poor mechanical behavior. Tensile tests can provide an answer to this question.

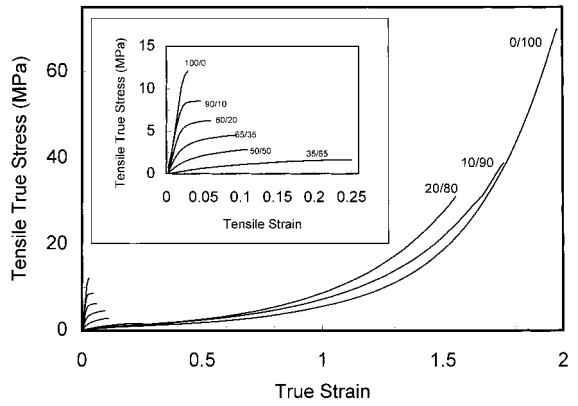

Figure 12. True stress vs true strain curves of PHB/PHO films at 25 °C, $d\epsilon/dt = 8.33 \times 10^{-3}$ s^{-1}. The compositions are indicated in the figure, and the insert is an expanded view of stress vs strain curves for PHB-rich films.

True stress vs True strain curves for PHB/PHO blends of 100/0 up to 0/100 at 25 °C are reported in Figure 12. At this temperature, PHB displays a brittle behavior, and it breaks for $\epsilon \approx 0.03$. With increasing PHO content, the material becomes more ductile, and two types of mechanical behavior are displayed for these films in Figure 12 depending on the composition. PHB-rich samples (up to 50 wt %) are characterized by a relatively high tensile modulus and a low ultimate strain. At higher PHO content, the blends display typical behavior of elastomeric materials. Whitening of the specimen was observed during tensile tests under large deformation. Usually in two-phase systems when one has weak

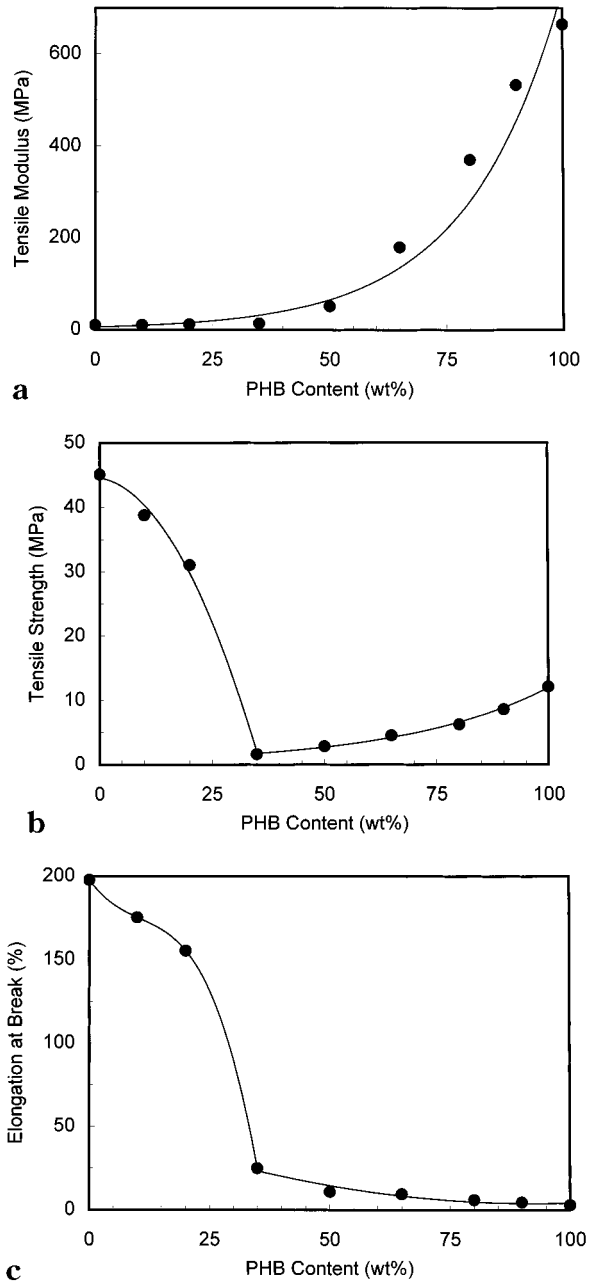

Figure 13. (a) Young's modulus, (b) tensile strength, and (c) elongation at break of PHB/PHO blends vs PHB content (the solid lines serve to guide the eye).

adhesion between the phases, one sees cavitation, which usually is seen as whitening. The tensile or Young's modulus was determined from the slope of the stress vs strain curves in the vicinity of $\sigma = \epsilon = 0$. Results are plotted in Figure 13, as well as the tensile strength and the elongation at break vs blend composition. Experimental data are also collected in Table 1. The tensile moduli are in agreement with storage tensile modulus values measured at room temperature (Figure 8a).

The tensile modulus, E, observed for PHB (665 MPa) agrees with what was reported in earlier studies (~1 GPa).[6,22,49] Tensile strength, σ_b, and ultimate strain, ϵ_b, values ranging from 28 to 68 MPa and from 1 to 5%, respectively, were reported.[6,22,26,49] These values are in agreement with our measurements, but it is well-known that the tensile behavior greatly depends on the experimental conditions, such as strain rate and temperature. The E, σ_b, and ϵ_b values observed for PHO (10.4 MPa, 45.1 MPa, and 198%, respectively) are in concordance with our previous results (13.1 MPa, 43.4 MPa, and 186%, respectively).[34] Gagnon et al. reported tensile modulus values ranging from 2.5 to 9 MPa,[33] depending on the crystallization temperature, which are lower than the one reported by Marchessault et al. (17 MPa).[50]

Table 1. Mechanical Properties of PHB/PHO Cast-films: Tensile Modulus, *E*, Tensile Strength, σ_b, and Ultimate Strain, ϵ_b

sample	E (MPa)	σ_b (MPa)	ϵ_b (%)
100/0	665	12.1	2.9
90/10	533	8.6	4.6
80/20	370	6.2	5.9
65/35	180	4.5	9.4
50/50	51.5	2.8	10.9
35/65	13.9	1.6	25.0
20/80	12.0	31.0	155
10/90	10.5	38.8	175
0/100	10.4	45.1	198

The Young's modulus increases significantly when the PHB concentration is increased from 50 up to 100 wt % (Figure 13a). The tensile strength first decreases rapidly as the PHB content increases up to a minimum value close to 2 MPa for the 35/65 blend (Figure 13b). At higher PHB concentration, σ_b increases slightly. The evolution of the ultimate strain vs PHB content (Figure 13c) also displays two distinct regions, namely below and above 35 wt %. These phenomena arise from an inversion phase. At low PHB concentration, PHO forms the matrix and the mechanical behavior of the material is governed by the theory of rubber elasticity. The tensile modulus is low, the elongation at break is high, and the high tensile strength is due to the orientation of the amorphous rubbery chains of the PHO matrix. At high PHB content, PHB forms the matrix and the mechanical behavior of the material is from enthalpic origin. The material displays a high tensile modulus, and a low ultimate strain. For intermediate concentration (35−50 wt % of PHB), PHO and PHB probably form co-continuous phases. The modulus value is very low, and the σ_b and ϵ_b values are very low too. This phenomenon is ascribed to a crazing effect or to a dewetting effect in which the adhesion between both parent polymers is destroyed, leading to a weakening of the interface strength. The lack of intimate adhesion between both components leads to numerous irregularly shaped microvoids or microflaws in the blend structure.

Modeling of the Tensile Behavior. To gain insight with regard to the tensile behavior of the PHB/PHO blends, the tensile modulus E can be predicted using the previous 3B model. The E value of the blend can be calculated using eq 1, in which the complex moduli are now real. E is plotted on a logarithm scale vs PHB content in Figure 14, for both the experimental and predicted data. Moreover, the behavior of the material in the case of weak adhesion (i.e., excluding the second term in eq 1, which corresponds to the two phases connected in series) and in the case of breakage of the rigid PHB phase (i.e., excluding the third term in eq 1, which corresponds to the continuous PHB phase) have been added. The modulus of the PHB/PHO blends in the case of both weak adhesion and breakage of the rigid PHB phase is also reported in Figure 14.

The presence or the lack of adhesion between both phases does not influence strongly the prediction above the critical volume fraction of PHB at the percolation threshold in the absence of breakage of the PHB phase.

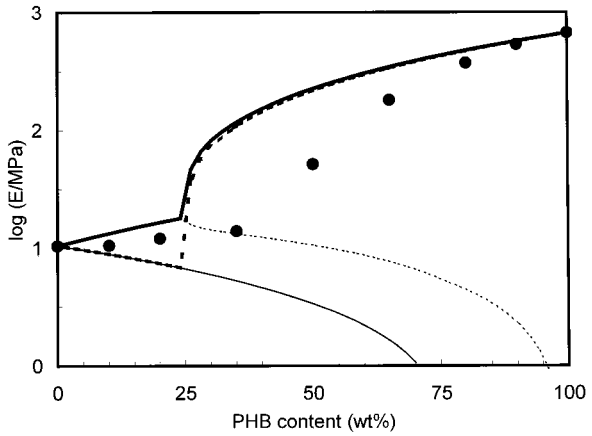

Figure 14. Experimental and predicted data for the logarithm of the tensile modulus vs PHB content: (●) experimental data, and predicted data for the case of complete 3B model (bold continuous line), for the case of nonadhesion between both phases (bold dashed line), for the case of rupture of the rigid PHB phase (thin dashed line), and for the case of both nonadhesion between phases and rupture of the rigid phase (thin continuous line).

This is due to the connectivity of PHB domains, which govern the mechanical behavior of the blend above this volume fraction. We ascertain that these two models (bold continuous line and bold dashed line) poorly fit the experimental data. As soon as a continuous PHB phase exists in the material, the prediction from these two models is systematically higher than the experimental modulus. Since dynamic mechanical analysis involves weak stresses, the adhesion between domains is not damaged. This explains why a good agreement for the unrelaxed and relaxed moduli was observed between prediction and experiment for all the materials. Under higher stress, as used for tensile tests, the adhesion is involved.

In addition, one can think that brittle PHB fractures as the strain increases. This situation can be accounted for by using the 3B model for the case of breakage of the rigid PHB phase. The predicted data agree roughly with experimental ones at low PHB content (up to 35 wt % PHB) but are lower for higher PHB compositions (Figure 14). The most convenient explanation is that both phenomena are involved in the experimental behavior. Therefore, in addition to weak adhesion between both components, the continuous PHB domains, if any, break partially under tensile solicitation.

Conclusion

Blends consisting of PHB and PHO prepared by solution blending were processed using chloroform as a common solvent. It may be concluded that PHB/PHO blends form a biphasic system over the whole composition range, with the phases consisting of the two pure polymers. This immiscibility was displayed by SEM, DSC and DMA analysis. In this two-phase system the nature of the continuous phase is composition-dependent and strongly influences the mechanical behavior of the blend. A model based on the percolation concept for the mechanical coupling between domains of polymer blends was used in both the linear and nonlinear range. It can take into account all types of morphologies (inclusions in a matrix, co-continuous phases, etc....). In addition, it allows for the effect of the lack of adhesion between material domains and/or breakage of one of the component.

Acknowledgment. The authors gratefully acknowledge Dr. E. Samain for PHO cultivation, Mr. D. Haase and Mrs. C. Juvin for their help in film processing, Mrs. D. Dupeyre for SEM, Mr. M. Paillet for its help in DSC measurements, and Mrs. C. Sprimont, Monsanto Europe S.A., for kindly supplying the samples of PHB.

Appendix

Calculation of the real and imaginary parts of the complex tensile modulus, according to the various models follows.

Voigt Model:

$$E' = v_O E'_O + (1 - v_O)E'_O$$
$$E'' = v_O E''_O + (1 - v_O)E''_O$$

Reuss Model:

$$E' = \{v_O(E'^2_H E'_O + E'^2_O E''^2_O + E'_H E''_H E''_O) + (1 - v_O)(E'_H E'^2_O + E'_H E''^2_O + E'_H E''_H E''_O)\}/\{[v_O E'_H + (1 - v_O)E''_O]^2 + [v_O E''_H + (1 - v_O)E''_O]^2\}$$

$$E'' = \{v_O(E'^2_H E''_O + E''^2_O E''^2_O + E'_H E'_O E''_H - E'_H E'_O E''_H) + (1 - v_O)(E'^2_O E''_H + E''_H E''^2_O + 2E'_H E'_O E''_O)\}/\{[v_O E'_H + (1 - v_O)E'_O]^2 + [v_O E''_H + (1 - v_O)E''_O]^2\}$$

Two Branch H (2BH) Model:

$$E' = \psi_H E'_H + (1 - \psi_H)^2\{v_O(E'^2_H E'_O + E'_O E''^2_H + E'_H E''_H E''_O) + (1 - v_O - \psi_H)(E'_H E''^2_O + E'_O E''_H E''_O)\}/\{[v_O E'_H + (1 - v_O - \psi_H)E'_O]^2 + [v_O E''_H + (1 - v_O - \psi_H)E''_O]^2\}$$

$$E'' = \psi_H E''_H + (1 - \psi_H)^2\{v_O(E'^2_H E''_O + E''^2_H E''_O + E'_H E'_O E''_H - E'_H E'_O E''_H) + (1 - v_O - \psi_H)(E'^2_O E''_H + E''_H E''^2_O + 2E''_H E'_O E''_O)\}/\{[v_O E'_H + (1 - v_O - \psi_H)E'_O]^2 + [v_O E''_H + (1 - v_O - \psi_H)E''_O]^2\}$$

Two Branch O (2BO) Model:

$$E' = \psi_O E'_O + (1 - \psi_O)^2\{(v_O - \psi_O)(E'^2_H E'_O + E'_O E''^2_H + E'_H E''_H E''_O) + (1 - v_O)(E'_H E'^2_O + E'_H E''^2_O + E'_O E''_H E''_O)\}/\{[(v_O - \psi_O)E'_H + (1 - v_O)E'_O]^2 + [(v_O - \psi_O)E''_H + (1 - v_O)E''_O]^2\}$$

$$E'' = \psi_O E''_O + (1 - \psi_O)^2\{(v_O - \psi_O)(E'^2_H E''_O + E''^2_H E''_O + E'_H E'_O E''_H - E'_H E'_O E''_H) + (1 - v_O)(E'^2_O E''_H + E''_H E''^2_O + 2E'_H E'_O E''_O)\}/\{[(v_O - \psi_O)E'_H + (1 - v_O)E'_O]^2 + [(v_O - \psi_O)E''_H + (1 - v_O)E''_O]^2\}$$

Three Branch (3b) Model:

$$E' = \psi_O E'_O + (1 - \psi_H - \psi_O)^2\{(v_O - \psi_O)(E'^2_H E'_O + E'_O E''^2_H + E'_H E''_H E''_O) + (1 - v_O - \psi_O)(E'_H E'^2_O + E'_H E''^2_O + E'_O E''_H E''_O)\}/\{[(v_O - \psi_O)E'_H + (1 - v_O - \psi_H)E'_O]^2 - [(v_O - \psi_O)E''_H + (1 - v_O - \psi_O)E''_O]^2\}$$

$$E'' = \psi_O E''_O + (1 - \psi_H - \psi_O)^2\{(v_O - \psi_O)(E'^2_H E''_O + E''^2_H E''_O + E'_H E'_O E''_H - E'_H E'_O E''_H) + (1 - v_O - \psi_H)(E'^2_O E''_H + E''_H E''^2_O + E'_H E'_O E''_O)\}/\{[(v_O - \psi_O)E'_H + (1 - v_O - \psi_H)E'_O]^2 + [(v_O - \psi_O)E''_H + (1 - v_O - \psi_O)E''_O]^2\}$$

References and Notes

(1) Greco, P.; Martuscelli, E. *Polymer* **1989**, *30*, 8, 1475.
(2) Kumagai, Y.; Doi, Y. *Polym. Degrad. Stab.* **1992**, *36*, 3, 241.
(3) Dubini Paglia, E.; Beltrame, P. L.; Canetti, M.; Seves, A.; Marcandalli, B.; Martuscelli, E. *Polymer* **1993**, *34*, 5, 996.
(4) Sadocco, P.; Canetti, M.; Seves, A.; Marcandalli, B.; Martuscelli, E. *Polymer* **1993**, *34*, 16, 3368.
(5) Azuma, Y.; Yoshie, N.; Sakurai, M.; Inoue, Y.; Chu Jo, R. *Polymer* **1992**, *33*, 22, 4763.
(6) Abe, H.; Matsubara, I.; Doi, Y. *Macromolecules* **1995**, *28*, 844.
(7) Kumagai, Y.; Doi, Y. *J. Environ. Polym. Degrad.* **1993**, *1*, 2, 81.
(8) Yoon, J. S.; Chang, M. C.; Kim, M. N.; Kang, E. J.; Kim, C.; Chin, I. J. *J. Polym. Sci., Part B: Polym. Phys.* **1996**, *34*, 2543.
(9) Marand, H.; Collins, M. *ACS Polym. Prepr.* **1990**, *31* (1), 552.
(10) Edie, S. L.; Marand, H. *ACS Polym. Prepr.* **1991**, *32* (2), 329.
(11) Scandola, M.; Ceccorulli, G.; Pizzoli, M. *Macromolecules* **1992**, *25*, 6441.
(12) Avella, M.; Martuscelli, E. *Polymer* **1988**, *29*, 1731.
(13) Kim, M. N.; Lee, A. R.; Lee, K. H.; Chin, I. J.; Yoon, J. S.. *Eur. Polym. J.* **1999**, *35*, 1153.
(14) Yoon, J. S.; Choi, C. S.; Maing, S. J.; Choi, H. J.; Lee, H. S.; Choi, S. J. *Eur. Polym. J.* **1993**, *29*, 10, 1359.
(15) Lotti, N.; Pizzoli, M.; Ceccorulli, G.; Scandola, M. *Polymer* **1993**, *34*, 23, 4935.
(16) Marchessault, R. H.; Bluhm, T. L.; Deslandes, Y.; Hamer, G. K.; Orts, W. J.; Sundararajan, P. R.; Taylor, M. G.; Bloembergen, S.; Holden, D. A. *Makomol. Chem., Macromol. Symp.* **1988**, *19*, 235.
(17) Kumagai, Y.; Doi, Y. *Polym. Degrad. Stab.* **1992**, *37*, 3, 253.
(18) Barham, P. J.; Barker, P.; Organ, S. J. *FEMS Microbiol. Rev.* **1992**, *103*, 289.
(19) Organ, S. J.; Barham, P. J. *Polymer* **1993**, *34*, 3, 459.
(20) Pearce, R. P.; Marchessault, R. H. *Macromolecules* **1994**, *27*, 3869.
(21) Gassner, F.; Owen, A. J. *Polym. Int.* **1996**, *39*, 215.
(22) Abbate, M.; Martuscelli, E.; Ragosto, G.; Scarinzi, G. *J. Mater. Sci.* **1991**, *26*, 1119.
(23) Verhoogt, H.; Ramsay, B. A.; Favis, B. D. *Polymer* **1994**, *35*, 24, 5155.
(24) Nijenhuis, A. J.; Colstee, E.; Grijpma, D. W.; Pennings, A. J. *Polymer* **1996**, *37*, 5849.
(25) Yoon, B. S.; Joang, J. Y.; Suh, M. H.; Lee, Y. M.; Lee, S.H. *Polym. Compos.* **1997**, *18*, 757.
(26) Gagnon, K. D.; Bain, D. B.; Lenz, R. W.; Fuller, R. C. In *Novel biodegradable microbial polymers*; Dawes, E. A., Ed.; Kluwer Academic Publishers: Dordrecht, The Netherlands, 1990; pp 449−450.
(27) Mallardé, D.; Valière, M.; David, C.; Menet, M.; Guérin, P. *Polymer* **1998**, *39*, 15, 3387.
(28) Morin, F. G.; Marchessault, R. H. *Macromolecules* **1992**, *25*, 576.
(29) Gross, R. A.; DeMello, C.; Lenz, R. W.; Brandl, H.; Fuller, R. C *Macromolecules* **1989**, *22*, 1106.
(30) Pearce, R.; Marchessault, R. H. *Polymer* **1994**, *35*, 18, 3990.
(31) Dubief, D.; Samain, E.;Dufresne, A. *Macromolecules* **1999**, *32*, 5765.
(32) Dufresne, A. Kellerhals, M. B.; Witholt, B. *Macromolecules* **1999**, *32*, 7396.
(33) Gagnon, K. D.; Lenz, R. W.; Farris, R. J.; Fuller, R. C. *Macromolecules* **1992**, *25*, 3723.
(34) Dufresne, A.; Samain, E. *Macromolecules* **1998**, *31*, 6426.
(35) Dufresne, A.; Etienne, S.; Perez, J.; Demont, P.; Diffalah, M. Lacabanne, C.; Martinez, J. J. *Polymer* **1996**, *37*, 12, 2359.
(36) Hashin, Z. *J. Appl. Mechan.* **1983**, *50*, 481.
(37) Takayanagi, M.; Uemura, S.; Minami, S. *J. Polym. Sci. C* **1964**, *5*, 113.
(38) Kerner, E. H. *Proc. Phys. Soc.* **1956**, *B69*, 808.
(39) Dickie, R. A. *J. Appl. Polym. Sci.* **1973**, *17*, 45.
(40) Lewis T. B.; Nielsen L. E. *J. Appl. Polym. Sci.* **1970**, *14*, 1449.
(41) Jourdan, C.; Cavaillé, J. Y.; Perez, J. *Polym. Eng. Sci.* **1988**, *28*, 1318.
(42) Ouali, N.; Cavaillé, J. Y.; Perez, J. *Plast. Rubber Compos. Process. Appl.* **1991**, *16*, 55.
(43) Garcia-Ramirez, M.; Cavaillé, J. Y.; Dufresne, A.; Tékély, P. *J. Polym. Sci., Polym. Phys.* **1995**, *33*, 2109.
(44) Dufresne, A.; Cavaillé, J. Y.; Dupeyre, D.; Garcia-Ramirez, M.; Romero, J. *Polymer* **1999**, 40, 7, 1657.
(45) Ferry, J. D. In *Viscoelastic Properties of Polymers*; John Wiley: New York, 1980.
(46) Garcia-Ramirez, M.; Cavaillé, J. Y.; Dufresne, A.; Dupeyre, D. *J. Appl. Polym. Sci.* **1996**, *59*, 1995.
(47) de Gennes, P. G. In *Scaling Concepts in Polymer Physics*; Cornell University Press: Ithaca, NY, 1979.
(48) Stauffer, D. In *Introduction to Percolation Theory*; Taylor and Francis: London and Philadelphia, PA, 1985.
(49) Koller, I.; Owen, A. J. *Polym. Int.* **1996**, *39*, 175.
(50) Marchessault, R. H.; Monasterios, C. J.; Morin, F. G.; Sundararajan, P. R. *Int. J. Biol. Macromol.* **1990**, *12*, 158.

MA991854A